Imbalances in Regional Lung Ventilation
A Validation Study on Electrical Impedance Tomography

Josué A. Victorino, João B. Borges, Valdelis N. Okamoto, Gustavo F. J. Matos, Mauro R. Tucci, Maria P. R. Caramez, Harki Tanaka, Fernando Suarez Sipmann, Durval C. B. Santos, Carmen S. V. Barbas, Carlos R. R. Carvalho, and Marcelo B. P. Amato

Respiratory ICU, Hospital das Clínicas, Pulmonary Department; General ICU, Hospital das Clínicas, Emergency Clinics Division; Radiology Department, Hospital das Clínicas, University of São Paulo, São Paulo, Brazil; and Department of Intensive Care, Fundación Jiménez Díaz, Madrid, Spain

Imbalances in regional lung ventilation, with gravity-dependent collapse and overdistention of nondependent zones, are likely associated to ventilator-induced lung injury. Electric impedance tomography is a new imaging technique that is potentially capable of monitoring those imbalances. The aim of this study was to validate electrical impedance tomography measurements of ventilation distribution, by comparison with dynamic computerized tomography in a heterogeneous population of critically ill patients under mechanical ventilation. Multiple scans with both devices were collected during slow-inflation breaths. Six repeated breaths were monitored by impedance tomography, showing acceptable reproducibility. We observed acceptable agreement between both technologies in detecting right–left ventilation imbalances (bias = 0% and limits of agreement = −10 to +10%). Relative distribution of ventilation into regions or layers representing one-fourth of the thoracic section could also be assessed with good precision. Depending on electrode positioning, impedance tomography slightly overestimated ventilation imbalances along gravitational axis. Ventilation was gravitationally dependent in all patients, with some transient blockages in dependent regions synchronously detected by both scanning techniques. Among variables derived from computerized tomography, changes in absolute air content best explained the integral of impedance changes inside regions of interest ($r^2 \geq 0.92$). Impedance tomography can reliably assess ventilation distribution during mechanical ventilation.

Keywords: artificial respiration; physiologic monitoring; validation studies; adult respiratory distress syndrome; respiratory insufficiency

Patients under artificial ventilation often present heterogeneous lung aeration, with inadequate distribution of V_T (1, 2). Prevalent conditions such as increased lung weight (3), lung compression by the heart (4, 5), abnormalities of chest wall (6, 7), and impaired surfactant function (8) promote not only a collapse of dependent lung zones, but also hyperdistention of nondependent zones (9–11). Such imbalances create zones of stress concentration inside the parenchyma, with increased risks for ventilator-induced lung injury (12).

Although global indexes of lung function like blood gases (13, 14), lung mechanics (15, 16), and plethysmography (17) have been used to track those ventilatory imbalances, they provide limited information. Imaging techniques such as magnetic resonance (18) or computerized tomography (CT) can provide better information about lung heterogeneities (14, 19–21), but they lack the dynamic features and bedside monitoring capabilities needed for intensive care.

Electrical impedance tomography (EIT) has emerged as a new imaging tool for bedside use (22–25). It is a noninvasive and radiation-free technique based on the measurement of electric potentials at the chest wall surface. Within a particular cross-sectional plane, harmless electrical currents are driven across the thorax in a rotating pattern, generating a potential gradient at the surface, which is then transformed into a two-dimensional image of the electric impedance distribution within the thorax.

Recent experimental studies have suggested that EIT images are very sensitive to regional changes in lung aeration (26–32). The dynamic behavior and the qualitative information extracted from EIT images look similar to that reported in dynamic CT studies (2, 33, 34) or in ventilation scintigraphy (31, 35). Its potential use as an online positive end-expiratory pressure titration tool has also been proposed, as EIT apparently provides reliable information about the recruitment/derecruitment of dependent lung regions (27, 28, 36, 37) and thus about the associated risk of ventilator-induced lung injury.

However, the poor spatial resolution of current EIT devices casts doubts on the promises mentioned previously here. As EIT does not keep perfect anatomic correspondence with CT images, we do not know yet whether we can translate the knowledge acquired from CT studies to the EIT universe. Although a recent animal study (38) suggested a good linear relationship between regional impedance changes and density changes (measured in Hounsfield units), we do not know how to use best the quantitative pixel information provided by EIT or how reliable it is in critically ill patients with acute lung injury.

We designed this study to answer the questions mentioned previously here and to test specifically whether EIT can consistently quantify ventilation imbalances caused by gravitational forces on the injured lung. We also tested whether some minimal anatomic/functional agreement with dynamic CT images can be obtained in critically ill patients. Part of this investigation has been previously reported in the form of abstracts (26, 39).

METHODS

Ten adult patients under mechanical ventilation were recruited (Table 1) after obtaining informed consent from patients' relatives.

Experimental Protocol

Dynamic sequences of EIT and CT scans, repeatedly at the same thoracic plane, during a slow-flow inflation maneuver were compared in supine patients. It was impossible to obtain simultaneous EIT and CT images because of excessive electromagnetic interference. Therefore, we performed three sets of slow inflations in the intensive care unit, monitored by EIT (DAS-01P, Sheffield, UK), followed by one set monitored

(*Received in original form January 30, 2003; accepted in final form December 18, 2003*)

Supported by the Fundação de Amparo à Pesquisa do Estado de São Paulo.

Correspondence and requests for reprints should be addressed to Marcelo Amato, M.D., Laboratório de Pneumologia, LIM09, Faculdade de Medicina da USP, Av Dr Arnaldo, 455 sala 2206 (2nd floor), CEP: 01246–903, São Paulo, SP, Brazil. E-mail: amato@unisys.com.br

This article has an online supplement, which is accessible from this issue's table of contents online at www.atsjournals.org

Am J Respir Crit Care Med Vol 169. pp 791–800, 2004
Originally Published in Press as DOI: 10.1164/rccm.200301-133OC on December 23, 2003
Internet address: www.atsjournals.org

TABLE 1. PATIENT CHARACTERISTICS AT ENTRY

Patient	Age	Sex	Diagnosis	APACHE II	Pa_{O_2}/FI_{O_2}	PEEP	VT (*ml*)	CST (*ml/cm H_2O*)	Days on Mechanical Ventilation
1	61	M	COPD, right lobectomy, sepsis	18	289	5	540	61	3
2	44	M	Stroke, alcohol abuse, sepsis	35	222	15	480	35	8
3	52	M	Hemothorax, sepsis, pneumonia	8	114	14	460	59	8
4	43	F	COPD, AIDS, PCP	15	176	15	500	60	3
5	36	M	AIDS, miliary tuberculosis, PCP	12	270	15	290	17	10
6	43	M	Histoplasmosis, tuberculosis	13	188	16	250	56	8
7	39	M	Pulmonary carcinoma, sepsis	22	192	18	400	17	9
8	36	M	Non-Hodgkin lymphoma, sepsis	11	237	20	350	47	4
9	60	F	Congestive heart failure, lung edema	22	240	15	500	68	8
10	31	M	Systemic lupus, miliary tuberculosis	19	227	13	370	22	20

Definition of abbreviations: APACHE II = Acute Physiology and Chronic Health Evaluation II; COPD = chronic obstructive pulmonary disease; CST = respiratory system compliance (average slope of the inflation pressure–volume curve, from zero to 30 cm H_2O); F = female; M = male; PCP = *Pneumocystis carini* pneumonia; PEEP = positive end-expiratory pressure.

The exclusion criteria were as follows: contraindications for sedation, paralysis, or hypercapnia, and presence of bronchopleural fistula.

by CT (GE HighSpeed, Milwaukee, WI). Back to the intensive care unit, three additional slow inflations were again monitored by EIT. By repeating EIT acquisition before and after patient transport to the CT room, we fully tested EIT reproducibility.

To start lung inflations from same approximate resting volume, lung history was homogenized before each one of the seven slow inflations by applying continuous positive airway pressure of 40 cm H_2O, lasting 20 seconds, followed by disconnection against atmosphere for 15 seconds.

The slow inflation was initiated by directing a constant flow generator (1 L/minute) toward the endotracheal tube through a three-way stopcock, linked in series to a proximal pressure/flow sensor. Data were sampled at 100 Hz. Inflation stopped at 45 cm H_2O, enough to obtain approximately 100 EIT scans (0.8 image/second) or 45 CT scans (0.3 image/second).

We always started the slow inflation 1.0 to 1.5 seconds before starting the first EIT or CT scan. Hardware scanning time was 1.0 second for both devices. Pressure/flow signals were continuously stored (100 Hz sampling) in a personal computer with its internal clock previously synchronized with EIT and CT machine clocks.

Electrode Positioning

For EIT measurements, 16 standard electrocardiograph electrodes were placed around the thorax at the transverse plane crossing the fifth intercostal space at midclavicular line. To check potential interferences of positioning of electrodes on image reconstruction (Figure 1), two different electrode-positioning arrangements were tested, exactly at the same transverse plane: (*1*) standard positioning—equally spaced—the distance between two adjacent electrodes kept constant along thoracic perimeter; the first electrode was always placed at sternum, and (*2*) test positioning—electrodes 5 (left armpit) and 13 (right armpit; Figure 1) were displaced upward (3 cm), closer to anterior axillary line. Interelectrode distances were evenly shortened on anterior thoracic surface and evenly expanded on posterior surface.

Electrode positioning for the first scan was randomly selected. The second scan was performed under the alternative positioning. For the third, no electrode replacements were made. The previous set of electrodes was completely removed whenever we changed electrode positioning or before transport to CT.

EIT Scans

The EIT device injected an alternating current (51 kHz, 2.1 root mean square [RMS]) between sequential pairs of adjacent electrodes. During each injection pattern, voltage differences between adjacent pairs of noninjecting electrodes were collected. The first scanning cycle worked as reference voltage set, with all image pixels (pixel = minimal element for image reconstruction) assigned to zero. Subsequently, new scanning cycles were collected every 1.2 seconds, each providing information to reconstruct one new relative image. By using a long scanning time (1 second), impedance changes were mostly related to changes in lung aeration, with negligible effects of perfusion waves (40–45). Each image represented the relative change in impedance distribution within the transverse section of the chest, from the first scan (right after starting slow inflation) to current scan. Images were reconstructed through a mathematic algorithm called back projection (46, 47), in which pixel values were expressed as percentage changes of local impedance, not providing any information about absolute values of tissue impedance. In its formulation, the algorithm assumes that voltages were collected from a nearly rounded section of the body, projecting its estimates of impedance changes over a 32×32 circular matrix. Customized software automatically extracted pixel information from regions of interest (ROIs) correspondent to those assigned on CT images (Figure 2).

CT Scans

After a new homogenizing maneuver, sequential CT slices (every 3 seconds, scanning time = 1 second) were taken during slow inflation without interruption and repeatedly at the same cross-sectional plane defined for EIT. The collimation was set at 10 mm.

From each image, we obtained frequency distributions of CT numbers corresponding to manually determined ROIs, according to the topography shown in Figure 2. A customized software converted regional CT histograms into three derived variables: mean density, gas/tissue ratio, and air content, according to published formulas (48, 49).

VT Volume Distribution and Statistical Analysis

Retrospectively, we looked at airway flow tracings, identifying the start of slow inflation (error of $\pm$ 0.02 seconds). Using synchronized time information, we referenced EIT or CT scans relative to this time origin. Off-line, we synchronized EIT and CT acquisitions by linearly interpolating EIT image data to the same points in time where we had CT scans, getting 30–45 synchronized images per inflation. Because we used constant-flow generator, lungs were inflated up to equivalent volumes for all matched images.

The relationship between CT and EIT variables was addressed by multiple linear regression. By taking only the first and the last matched images, we calculated the relative distribution of VT across the ROIs. For CT, the percentage of tidal ventilation directed toward a particular ROI was calculated as the increment in air content for that ROI divided by the air content increment for the entire slice. For EIT, we took the last image and calculated the integral of pixel value over that corresponding ROI (50, 51) divided by integral of pixel value over the whole slice. Based on these estimates—presented as dimensionless numbers or percentages—we tested EIT reproducibility (comparing EIT estimates before versus after CT scan) and EIT versus CT agreement according to the principles proposed by Bland and Altman (52). Additional details are provided in the online supplement.

RESULTS

Stability of Lung Mechanics along the Study

Cross correlations among the seven pressure–time curves obtained for each patient were calculated. Because patient 2 presented at least one correlation coefficient of less than 0.9, inter-

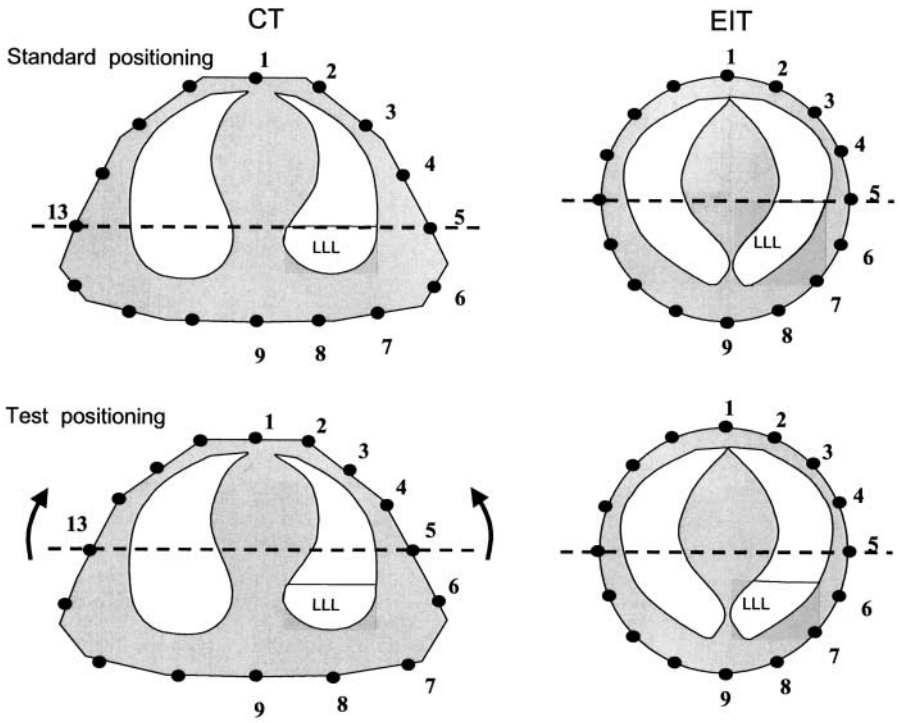

Figure 1. Sketch of thoracic plane and theoretic effects of different electrode positioning. During electrical impedance tomography (EIT) imaging, impedance changes occurring in real trapezoid domain (*left*) are projected over a circular EIT domain (*right*), deforming lung areas. The perimeter of the *EIT circle* necessarily corresponds to the skin with electrodes. By using standard electrode positioning (*top*), midelectrode 5 is frequently placed over the skin close the posterior lung (LLL illustrates an atelectatic left lower lobe) and not at midlung height. Because the EIT imaging algorithm assumes that electrode 5 is at midthoracic height, midway between electrodes 1 and 9, there is some shrinking of nondependent lung representation, with expansion of LLL. This is because EIT back projection assumes that every lung tissue above electrode 5 must be projected over the anterior part of the circular EIT representation, whereas every tissue below electrode 5 (LLL) has to occupy the whole posterior part of the circular EIT representation. The test positioning used in this study is illustrated at the bottom. Electrode 5 is displaced ventrally (3 cm), closer to midlung height. Electrodes 1–5 have now a shorter interelectrode distance than electrodes 5–9 (where subcutaneous tissue is abundant). We hypothesized that such positioning would avoid the overrepresentation of LLL.

preted as a signal of poor stability of lung mechanics across the measurements, he was excluded from subsequent analysis. Although discarded, the dynamics of lung inflation in this case was illustrative of the spatial resolution of EIT (being presented in the animations 1 and 2 in the online supplement).

Reproducibility

Reproducibility in EIT estimates of V_T distribution was assessed by calculating the within-subject SD between repeated measures (53). For each ROI, we calculated within-subject SD between repeated measures and bias observed between two consecutive

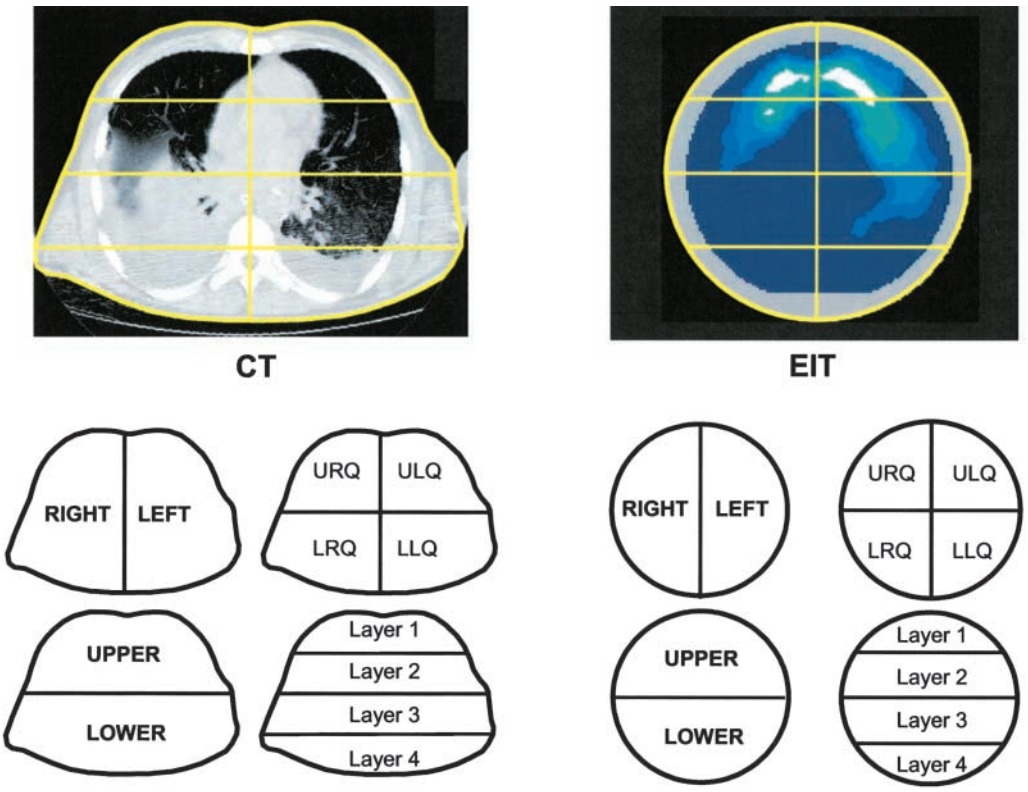

Figure 2. Schematic regions of interest (ROIs) on computerized tomography (CT) and EIT. Each of the 12 ROIs embraced a portion of the chest wall plus part of the lung. On EIT images, the portions were selected automatically by special software splitting the original circle with 788 pixels into subsets shown. On the CT image, the skin border was manually designed, forming the outer boundary of a cross-section of the thorax with approximately 140,000 pixels. Subsequently, uppermost and lowest pixels of contour were taken as references, and four evenly spaced layers, each one corresponding to one fourth of anteroposterior thoracic diameter, were drawn. Similarly, the crossing between skin contour and the horizontal line at midthoracic height defined references to split the thorax in its middle (*left and right halves*). URQ = upper right quadrant; ULQ = upper left quadrant; LRQ = lower right quadrant; LLQ = lower left quadrant.

measurements, always under the same electrode positioning. Considering all ROIs and both electrode-positioning arrangements together, we observed a global within-subject SD between repeated measures of 4.9% when electrodes were kept in place and 7.4% when we replaced electrode array after CT (separately considered: 7.0% for standard and 7.7% for test positioning). This demonstrates that replacement of electrodes increased random errors in our measurements. The bias was less than 1% for all situations. All of these results were below our a priori reproducibility cutoff of 9%.

Agreement

Agreement in estimates of V_T distribution according to EIT versus CT is presented in Figure 3. Even smaller ROIs presented acceptable agreement (i.e., sample limits of agreement did not exceed the boundaries established a priori) for either electrode positioning. Agreement was better for right–left imbalances than for upper–lower imbalances in ventilation. The worst agreement was observed in layer 1, with standard positioning (bias = +9.4% and sample limits of agreement = −6.4 to 25%).

Translating this agreement into images, Figure 4 exemplifies typical EIT images—contrasted with synchronized CT images.

Relative Distribution of V_T according to EIT and CT

Figure 5 shows the distribution of ventilation according to the horizontal and vertical axes in CT and EIT images. When considering potential imbalances between right/left fields, EIT and CT exhibited comparable estimates for regional ventilation (bias = 0% and limits of agreement = −10 to 10%, p = 0.31; Figure 5, left). Pooled measurements across patients suggested a rather homogeneous (approximately equal to 1:1) distribution of ventilation between right/left fields. However, there were some outliers, exemplified by patient 8 (Figure 4A), who had a solid mass entirely blocking the right lung and who obtained an estimate of ventilation toward the right field = 2% in CT analysis versus −3% in EIT analysis. CT and EIT similarly detected all outliers.

Likewise, both techniques detected equivalent imbalances when the upper and lower parts of the thorax were considered (upper/lower ratio = 82%/18% and 75%/25% for EIT and CT, respectively), also with a good case-by-case match. The overall inhomogeneity between the upper/lower fields was marginally larger with EIT (considering the standard electrode positioning) than with CT (p = 0.04).

Similarly to CT, EIT detected a large vertical gradient of regional ventilation across the four superimposed layers in all patients. The standard positioning of electrodes caused a slight overestimation of regional ventilation to layer 1, underestimating the ventilation to layer 3. The test positioning partially corrected this distortion (Figure 6).

Multiple regression analysis (Figure 7) further checked two potential errors in EIT analysis: (*1*) image distortions and (*2*) a lack of linear relationship between electrical properties versus density (X-ray attenuation) of tissues. We assumed CT based variables as "gold standard" (independent variables), intentionally plotting the entire data sequence for all regions together, in the same X–Y plane. We reasoned that both potential errors were expected to compromise the overall coefficient of determination. This is because EIT image distortions tend to produce plots with different slopes for each region. For instance, consider an EIT slice with adjacent regions, A and B. Consider also the x axis representing true changes in air content for regions A or B (measured by CT) versus the y axis representing the measured changes in impedance. If part of a true impedance change in region A was wrongly projected over region B (characterizing an image distortion), the slope of plot A would decrease, whereas

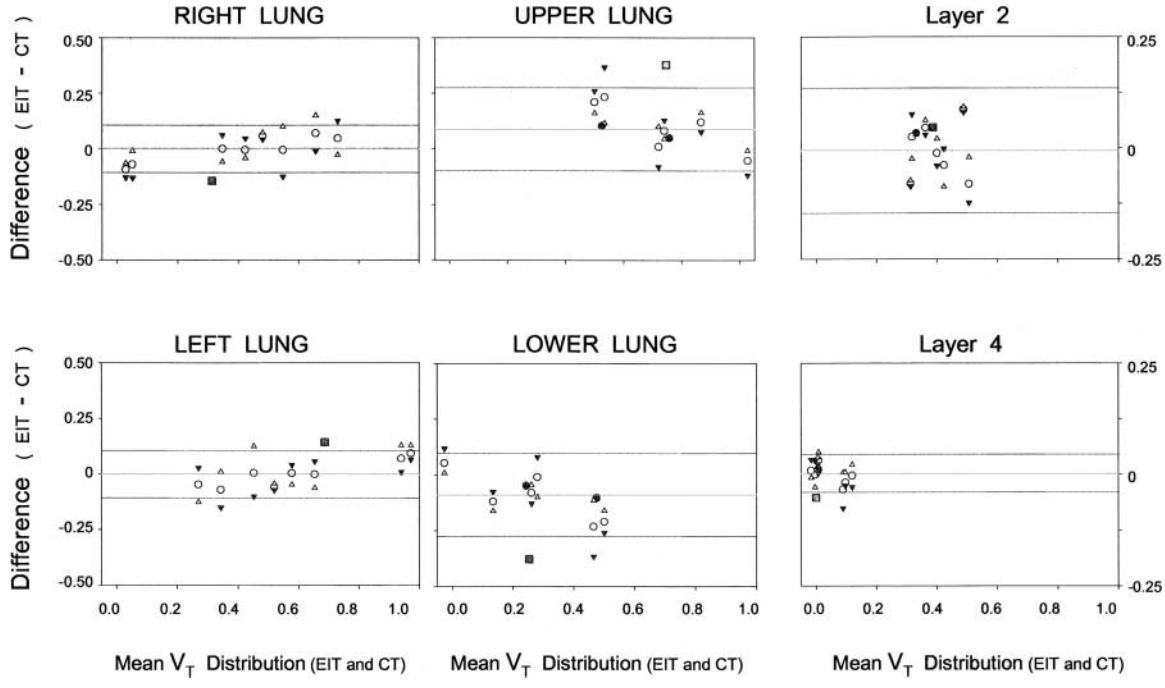

Figure 3. Bland-Altman plots of the differences in regional distribution of V_T estimated by EIT and CT (for brevity, only six representative lung regions, and only the standard electrode positioning is presented). The overall span of Y axis represents our a priori limits of agreement. (*Dotted lines*) Limits of agreement of the observed sample. (*Gray line*) Mean of observed differences. (*Downward triangles*) Measurements taken before CT exam. (*Upward triangles*) Measurements taken after CT exam. (*Circles*) The average difference. (*Gray square*) Patient 9, presenting acute cardiogenic pulmonary edema soon after CT scan, resulting in the largest disagreement.

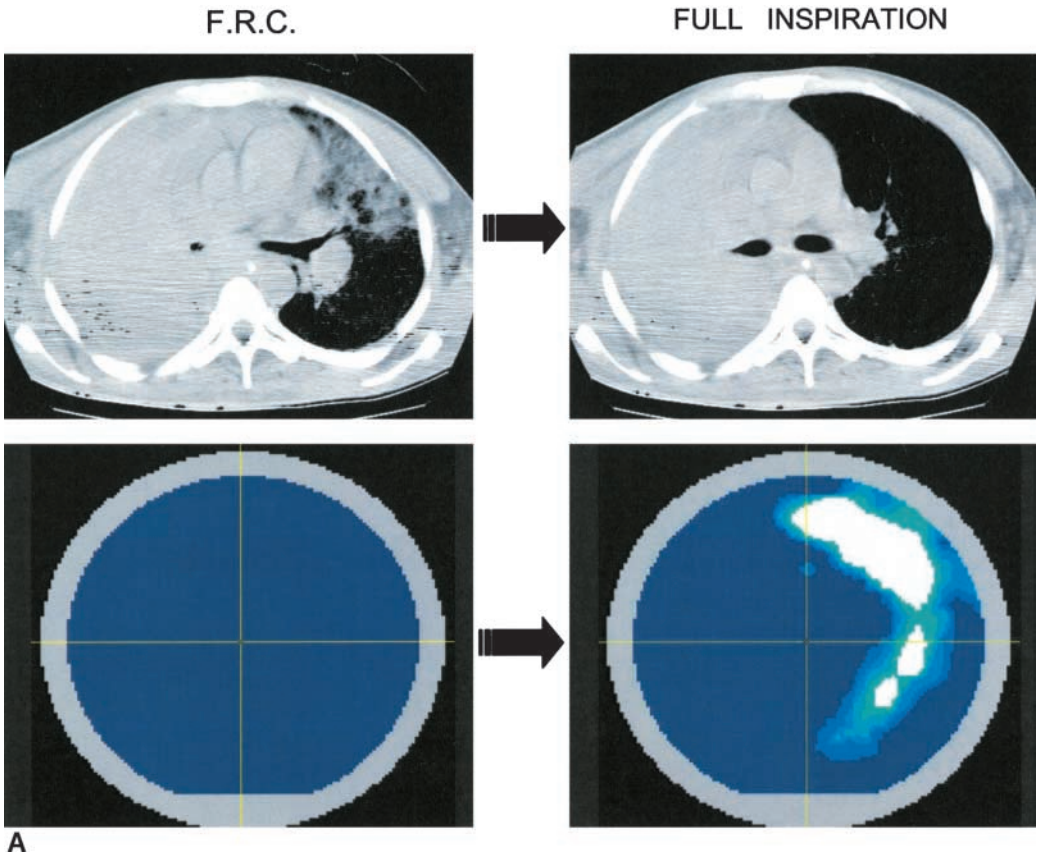

Figure 4. EIT and CT images obtained at start (*left*) and at end (*right*) of slow-inflation maneuver in patients 8 (*A*) and 3 (*B*). All CT images were obtained at the same thoracic plane (fifth intercostal space), which coincides with the plane of electrodes. The relative EIT images express only *variations* in impedance. Note that the back-projection algorithm projects impedance changes (*bright colors* represent increased impedance) onto the same quadrants suffering higher aeration in CT images (regions getting *darker shades of gray*). Atelectatic zones, the mediastinum, and the pleural effusion zones remain silent. F.R.C.= functional residual capacity.

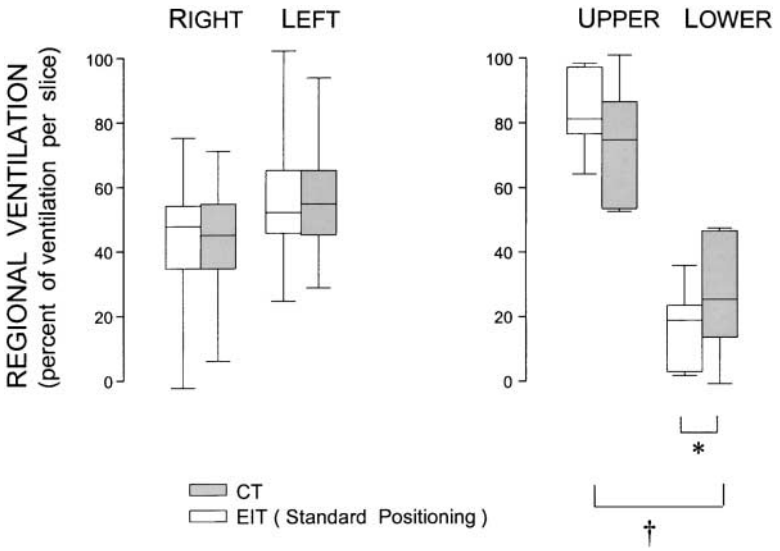

Figure 5. Box plot representing distributions of VT estimated by EIT (*white boxes*) and CT (*gray boxes*) in nine patients when using standard electrode positioning. *Boxes* indicate 25% and 75% percentiles, with the median line inside. *Error bars* represent 5% and 95% percentiles. The *left panel* points out ventilation imbalances between left and right thoracic areas. The *right panel* points out imbalances between upper and lower parts of the thorax. *p = 0.04 using asymptotic approximation for Wilcoxon Signed-rank test. †p = 0.02 using asymptotic approximation for Wilcoxon Signed-rank test.

the slope of plot B would increase in the same system of coordinates. The result would be a poor r^2.

Figure 7 shows that air content in CT presented best coefficient of determination ($r^2 = 0.92$, standard positioning; $r^2 = 0.93$, test positioning, data not shown) to predict regional impedance changes. Linear plots for each region were consistently observed, with very similar slopes across regions and patients. The same was not true for the relationships with the CT mean density ($r^2 = 0.57$) or with the gas/tissue ratio ($r^2 = 0.56$), where different slopes for each region compromised the overall coefficient of determination.

A common phenomenon observed in our patients was illustrated in Figure 8. Dependent lung zones presented transient blockage of regional ventilation at the beginning of slow infla-

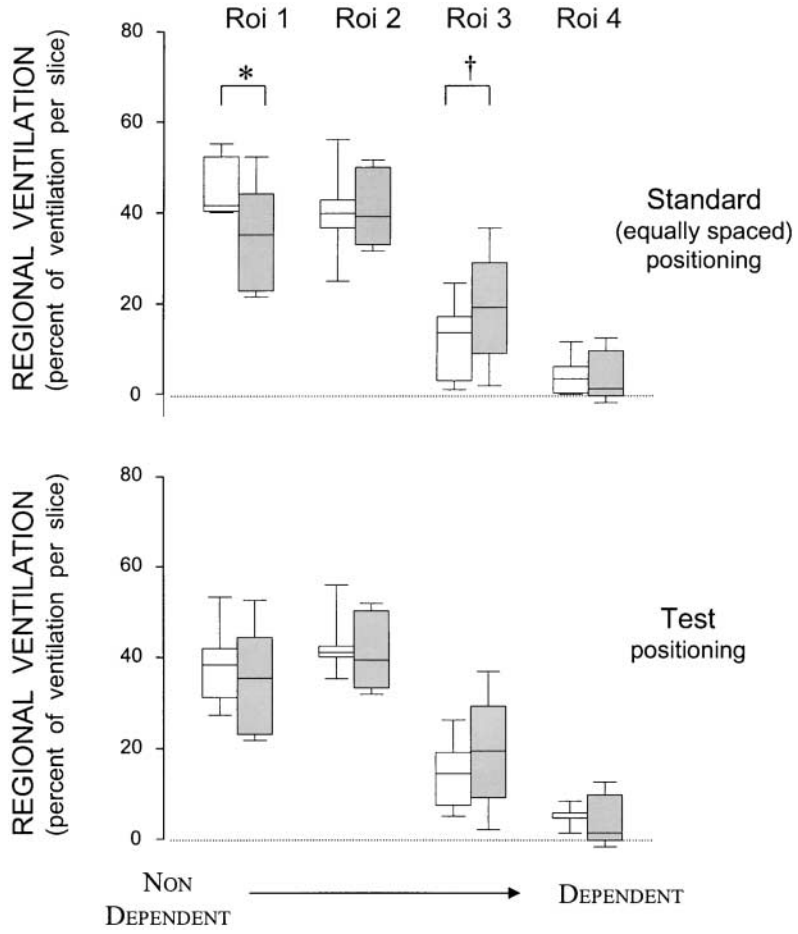

Figure 6. Box plot representing distributions of VT estimated by EIT (*white boxes*) and CT (*gray boxes*). Electrode positioning was standard in the *top* and test in the *bottom*. *Boxes* represent 25 and 75 percentiles, with the median line inside. *Error bars* represent 5 and 95 percentiles. There is an overall trend for progressively lower ventilations from ROI 1 to ROI 4, either in EIT (p = 0.001, Friedman test) or in CT (p = 0.003). The test positioning of electrodes resulted in better match with CT. Significant differences between CT and EIT estimates were detected only for the standard positioning. *p = 0.018 using asymptotic approximation for Wilcoxon Signed-rank test; †p = 0.028 using asymptotic approximation for Wilcoxon signed-rank test.

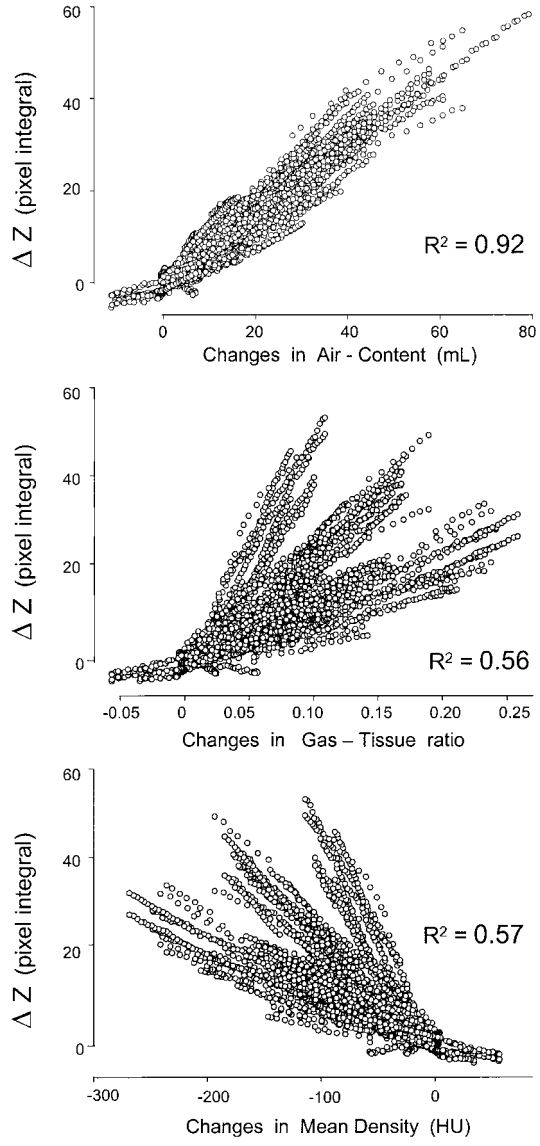

Figure 7. Scattered plots illustrating adjusted multiple regression for local impedance changes during slow inflation (standard electrode positioning) when projected over synchronized changes in CT images. Dependent variable in each plot represents integral of pixel values over a certain ROI in EIT, calculated for each image in the inflation sequence. Independent variables are, respectively, regional air content (*top*), regional gas/tissue ratio (*middle*), and regional mean density (*bottom*), all calculated from corresponding ROIs in CT images. Plots for all ROIs, patients, and trials (pre-or post-CT) are superposed, with approximately 9,600 data points per graph. r^2 represents within-subject coefficient of determination.

tion, although there was no visible collapse on CT at the start of slow inflation. After varied periods of time, this blockage was overcome, and the slope of impedance changes along time line suddenly increased in dependent zones, synchronously with the sudden increase in air content in dependent zones of CT slices.

DISCUSSION

The major findings in this study can be summarized as follows: (*1*) EIT images from patients under controlled mechanical ventilation were reproducible and presented good agreement to dynamic CT scanning. (*2*) Electrode array replacement slightly deteriorated the reproducibility of EIT measurements and the interelectrode spacing within the array affected the agreement with CT. (*3*) Although EIT estimates of right/left imbalances in regional lung ventilation were more precise (and less dependent on interelectrode spacing), gravity-related imbalances of regional lung ventilation could be reliably assessed, even for layers corresponding to one-fourth of anteroposterior thoracic distance; and (*4*) Regional impedance changes in the EIT slice were best explained by the corresponding changes in air content detected in the CT slice (explaining 92–93% of its variance). Other CT-derived variables, such as regional X-ray mean density or regional gas–tissue ratio, did not parallel regional changes in impedance as consistently.

An important methodologic aspect of this study is linked to the results discussed previously here: We used the integral of pixel values over each ROI—instead of simple pixel average—to represent the regional changes in impedance. There are several advantages with this approach. First, some bench tests using back-projection reconstruction have demonstrated the superior consistency of this parameter to quantify impedance perturbations all over the image slice—independently of its radial position (50, 51). Second, it allows the estimation of the percentage of V_T directed toward a particular ROI by simply calculating a normalized ratio (i.e., the integral over the ROI divided by the integral over the whole slice). This approach obviously decreases the between-patient variability. Finally, there was a strong rationale supporting this approach, particularly for our study, as explained later here. Because clear anatomic marks were absent in EIT images, we adopted a reproducible procedure for ROI delineation, independently of investigator or individual anatomy: We embraced structures suffering aeration together with structures that were not (e.g., the chest wall; Figure 2). Thus, the amount of nonexpandable tissue (with fixed localized impedance) necessarily attenuated the mean impedance change inside each ROI—in the same manner that they attenuated mean density changes on CT. However, the same attenuation is not expected to occur in the integral of pixel values. Varied amounts of compact tissue do not affect calculations for air content in CT analysis (because their calculations are not based on average values, but ultimately on the sum of pixel values), and similar results must be expected for the integral of EIT pixel values.

When estimating air content for each pixel in CT, we calculate the absolute amount of air contained in the voxel (voxel = minimum volume element to construct the image). The idea that the sum of these estimates produces a reliable number expressing air content inside the whole slice is intuitive. However, the understanding of how pixel values in EIT—expressed as percent changes in impedance—can be summed to estimate global changes in air content is not trivial. Recently, Nopp and colleagues (45) provided a theoretic framework supporting this convenient relationship, which was explored in this study as well as in a recent publication (54). Using an appropriate mathematic model for the alveolar structure and boundary conditions—like an almost invariant interstitial space along inspiration (i.e., constant tissue volume within the slice), projected over the same image pixels, and suffering moderate impedance changes (less than 100%)—the author demonstrated that each percentage change in pixel impedance should parallel absolute increments in air content for that corresponding parenchymal region, no matter the initial value for absolute resistivity in that region.

It follows that the integral of pixel value in EIT should parallel changes in air content, as calculated in CT slices. However, the same rationale does not stand for gas/tissue ratio (%) or CT mean densities (Hounsfield units), as suggested previously here: Different amounts of compact tissue across different ROIs are ex-

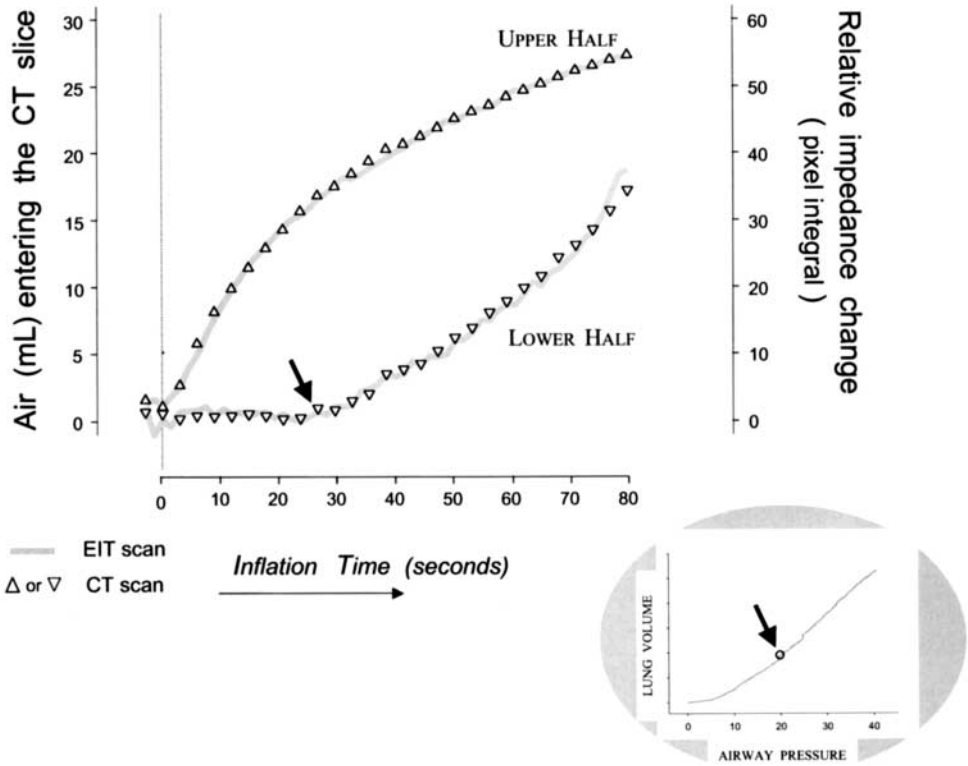

Figure 8. Temporal sequence of EIT and CT estimates during slow lung inflation. The *arrow* indicates the moment when the lower half of the thorax started to ventilate, almost 30 seconds later than the upper thorax.

pected to cause a poor correlation between EIT and these two latter CT variables. Figure 7 corroborates this hypothesis.

This stronger association with CT air content was a key finding in our study. Recently, Frerichs and colleagues (38) reported acceptable correlations between local impedance changes versus local changes in CT mean densities (in Hounsfield units). However, even using a less noisy EIT device in a controlled environment (they used normal pigs with convenient rounded thoracic geometry instead of patients with diseased lungs and trapezoid thoracic shapes), they reported lower coefficients of determination (ranging from 0.56 to 0.86). Methodologic differences such as their subjective ROI demarcations and the use of pooled regression, instead of a more appropriate within-subject regression (55), make any comparison difficult. However, altogether, those findings suggest that the choice for better parameters quantifying aeration in CT or EIT is essential for fair comparisons between both technologies or also to extract the most reliable information from EIT.

Limitations of This Study

Unlike the gold standard two-dimensional CT slice, with a homogenous thickness of 1 cm, EIT slice represents a less precise thickness of tissue, which is radius dependent (56). Part of the electrical current commonly flows through planes above and below the electrode plane, and the central part of the image is especially susceptible to these out of plane influences, theoretically up to 10 cm above or below. Therefore, an ideal comparison study should examine EIT against a thicker CT slicing (10–20 cm), requiring more radiation and multislice tomography.

Nevertheless, the high within-subject coefficient of determination obtained with our dynamic single-slice approach ($r^2 \geqslant 0.92$) suggests that even CT multislicing might not provide much additional information. One possible explanation for this finding is that in spite of theoretic assumptions, the amount of out of plane current may be negligible in the human thorax. Another important consideration is that the lung may be relatively homogeneous along the craniocaudal axis, behaving like a liquid body in patients under mechanical ventilation (57). By assuming this isogravitational behavior, out of plane changes would be similar to in-plane ones, minimally affecting our analysis (58).

Another limitation of our study might be related to the fact that EIT and CT acquisitions were not simultaneous and that the lung might behave slightly differently during each slow inflation (59). We tried to minimize this problem, contemplating procedures like the exclusion of nonreproducible pressure–time tracings, the averaging of two EIT acquisitions (before and after CT) for agreement analysis, and the use of intense homogenizing maneuvers before each slow inflation. Nevertheless, this intrinsic limitation eventually precluded us from obtaining better agreement with CT slices.

Our final concern is that the presented results are only valid for the specific device tested here and for ROIs not smaller than one-fourth of the thoracic cross-sectional area. These issues are linked, as technologic improvements such as new image reconstruction algorithms (60–67), larger number of electrodes (68), or higher precision in current injection or voltage readings could all decrease errors in EIT imaging, improving spatial resolution (69, 70). In fact, our reproducibility analysis suggests that we are close to the resolution limits of the tested device and that any further decrease in ROI size would impair reproducibility. As shown in this study, small differences in interelectrode spacing along the thoracic perimeter can have an impact on EIT analysis (Figure 6). Better electrode-array handling (71) and new mathematic formulations to take into account thoracic asymmetries are needed for the next years.

Implications of Current Data

Despite the limitations cited previously here, we think that the reported performance of EIT was good enough for certain clinical applications, especially bedside adjustments of mechanical

ventilation with immediate feedback. A similar EIT device could easily detect selective intubation, large pneumothorax, or lobar atelectasis. Additionally, as already reported by our group and others, subtle changes in the positive end-expiratory pressure level can produce large imbalances in regional ventilation along the gravity axis, usually by the same order of magnitude observed in this study (27, 36).

Despite the low spatial resolution of current EIT devices, the high temporal resolution of EIT looks promising. In our study, technical limitations forced us to use slow-motion inflation of the lung, which in turn allowed us to detect transient and usually imperceptible phenomena occurring during normal tidal breaths. For instance, dependent zones in most patients presented complete blockage of ventilation during significant part of inspiration (Figure 8). Suddenly, 20–30 seconds later, some regional ventilation could be precisely and simultaneously detected by EIT and CT—without detectable perturbation in simultaneous pressure–time tracings. The clinical relevance of such "inflation delays" is a matter for future studies, but faster temporal resolutions in new EIT devices would allow us to monitor such phenomena without any especial maneuver. In the context of evidences suggesting deleterious effects of tidal recruitment (72, 73), such sensitive detection at bedside is encouraging (26).

In conclusion, even at its current stage of development, EIT can reliably assess imbalances in distribution of V_T in critically ill patients. When comparing regional ventilation across different thoracic regions, the quantitative information provided by EIT carries good proportionality to changes in air content—as calculated by dynamic CT scanning—but not with CT gas/tissue ratio or CT mean densities.

Conflict of Interest Statement: J.A.V. has no declared conflict of interest; J.B.B. has no declared conflict of interest; V.N.O. has no declared conflict of interest; G.F.J.M. has no declared conflict of interest; M.R.T. has no declared conflict of interest; M.P.R.C. has no declared conflict of interest; H.T. has no declared conflict of interest; F.S.S. has no declared conflict of interest; D.C.B.S. has no declared conflict of interest; C.S.V.B. has no declared conflict of interest; C.R.C.C. has no declared conflict of interest; M.P.B.A. has no declared conflict of interest.

Acknowledgment: The authors thank the EIT Study Group (especially Professor Raul Gonzalez and the team of the Polytechnic Institute and Dr. Joyce Bevilacqua from the Applied Mathematics Institute, University of São Paulo) for their valuable input, criticisms, and discussions during the experiments and data analysis.

References

1. Gattinoni L, Mascheroni D, Torresin A, Marcolin R, Fumagalli R, Vesconi S, Rossi GP, Rossi F, Baglioni S, Bassi F, *et al.* Morphological response to positive end expiratory pressure in acute respiratory failure: computerized tomography study. *Intensive Care Med* 1986;12: 137–142.
2. Gattinoni L, D'Andrea L, Pelosi P, Vitale G, Pesenti A, Fumagalli R. Regional effects and mechanism of positive end-expiratory pressure in early adult respiratory distress syndrome. *JAMA* 1993;269:2122–2127.
3. Pelosi P, D'Andrea L, Vitale G, Pesenti A, Gattinoni L. Vertical gradient of regional lung inflation in adult respiratory distress syndrome. *Am J Respir Crit Care Med* 1994;149:8–13.
4. Malbouisson LM, Busch CJ, Puybasset L, Lu Q, Cluzel P, Rouby JJ. Role of the heart in the loss of aeration characterizing lower lobes in acute respiratory distress syndrome: CT Scan ARDS Study Group. *Am J Respir Crit Care Med* 2000;161:2005–2012.
5. Albert RK, Hubmayr RD. The prone position eliminates compression of the lungs by the heart. *Am J Respir Crit Care Med* 2000;161:1660–1665.
6. Pelosi P, Cereda M, Foti G, Giacomini M, Pesenti A. Alterations of lung and chest wall mechanics in patients with acute lung injury: effects of positive end-expiratory pressure. *Am J Respir Crit Care Med* 1995;152: 531–537.
7. Ranieri VM, Brienza N, Santostasi S, Puntillo F, Mascia L, Vitale N, Giuliani R, Memeo V, Bruno F, Fiore T, *et al.* Impairment of lung and chest wall mechanics in patients with acute respiratory distress syndrome: role of abdominal distension. *Am J Respir Crit Care Med* 1997; 156:1082–1091.
8. Lewis JF, Jobe AH. Surfactant and the adult respiratory distress syndrome. *Am Rev Respir Dis* 1993;147:218–233.
9. Vieira SR, Puybasset L, Richecoeur J, Lu Q, Cluzel P, Gusman PB, Coriat P, Rouby JJ. A lung computed tomographic assessment of positive end-expiratory pressure-induced lung overdistension. *Am J Respir Crit Care Med* 1998;158:1571–1577.
10. Gattinoni L, Pesenti A, Bombino M, Baglioni S, Rivolta M, Rossi F, Rossi G, Fumagalli R, Marcolin R, Mascheroni D, *et al.* Relationship between lung computed tomographic density, gas exchange, and PEEP in acute respiratory failure. *Anesthesiology* 1988;69:824–832.
11. Dambrosio M, Roupie E, Mollet JJ, Anglade MC, Vasile N, Lemaire F, Brochard L. Effects of positive end-expiratory pressure and different V_Ts on alveolar recruitment and hyperinflation. *Anesthesiology* 1997; 87:495–503.
12. Amato MBP, Marini JJ. Barotrauma, volutrauma, and the ventilation of acute lung injury. In: Marini JJ, Slutsky AS, editors. Physiological basis of ventilatory support, 1st ed. New York: Marcel Dekker; 1998. p. 1187–1245.
13. Hedenstierna G, Tokics L, Strandberg A, Lundquist H, Brismar B. Correlation of gas exchange impairment to development of atelectasis during anaesthesia and muscle paralysis. *Acta Anaesthesiol Scand* 1986;30: 183–191.
14. Malbouisson LM, Muller JC, Constantin JM, Lu Q, Puybasset L, Rouby JJ. Computed tomography assessment of positive end-expiratory pressure-induced alveolar recruitment in patients with acute respiratory distress syndrome. *Am J Respir Crit Care Med* 2001;163:1444–1450.
15. Katz JA, Ozanne GM, Zinn SE, Fairley HB. Time course and mechanisms of lung-volume increase with PEEP in acute pulmonary failure. *Anesthesiology* 1981;54:9–16.
16. Bryan AC, Milic-Emili J, Pengelly D. Effect of gravity on the distribution of pulmonary ventilation. *J Appl Physiol* 1966;21:778–784.
17. Brazelton TB III, Watson KF, Murphy M, Al-Khadra E, Thompson JE, Arnold JH. Identification of optimal lung volume during high-frequency oscillatory ventilation using respiratory inductive plethysmography. *Crit Care Med* 2001;29:2349–2359.
18. Tusman G, Böhm SH, Tempra A, Melkun F, Garcia E, Turchetto E, Mulder PGH, Lachmann B. Effects of recruitment maneuvers on atelectasis in anesthetized children. *Anesthesiology* 2003;98:14–22.
19. Puybasset L, Cluzel P, Gusman P, Grenier P, Preteux F, Rouby JJ. Regional distribution of gas and tissue in acute respiratory distress syndrome: I: consequences for lung morphology: CT Scan ARDS Study Group. *Intensive Care Med* 2000;26:857–869.
20. Brismar B, Hedenstierna G, Lundquist H, Strandberg A, Svensson L, Tokics L. Pulmonary densities during anesthesia with muscular relaxation: a proposal of atelectasis. *Anesthesiology* 1985;62:422–428.
21. Gattinoni L, Pelosi P, Crotti S, Valenza F. Effects of positive end-expiratory pressure on regional distribution of V_T and recruitment in adult respiratory distress syndrome. *Am J Respir Crit Care Med* 1995;151: 1807–1814.
22. Barber DC, Brown BH. Applied potential tomography. *J Phys E Sci Instrum* 1984;17:723–733.
23. Brown BH, Barber DC, Seagar AD. Applied potential tomography: possible clinical applications. *Clin Phys Physiol Meas* 1985;6:109–121.
24. Adler A, Shinozuka N, Berthiaume Y, Guardo R, Bates JH. Electrical impedance tomography can monitor dynamic hyperinflation in dogs. *J Appl Physiol* 1998;84:726–732.
25. Adler A, Amyot R, Guardo R, Bates JH, Berthiaume Y. Monitoring changes in lung air and liquid volumes with electrical impedance tomography. *J Appl Physiol* 1997;83:1762–1767.
26. Borges JB, Okamoto VN, Tanaka H, Janot GF, Victorino JA, Tucci MR, Carvalho CRR, Barbas CSV, Amato MBP. Bedside detection of regional opening/closing pressures by electrical impedance vs. computed tomography (CT) [abstract]. *Am J Respir Crit Care Med* 2001; 163:A755.
27. Kunst PW, Vazquez de Anda G, Bohm SH, Faes TJ, Lachmann B, Postmus PE, de Vries PM. Monitoring of recruitment and derecruitment by electrical impedance tomography in a model of acute lung injury. *Crit Care Med* 2000;28:3891–3895.
28. Kunst PW, Bohm SH, Vazquez de Anda G, Amato MB, Lachmann B, Postmus PE, de Vries PM. Regional pressure volume curves by electrical impedance tomography in a model of acute lung injury. *Crit Care Med* 2000;28:178–183.
29. Frerichs I, Hahn G, Schroder T, Hellige G. Electrical impedance tomography in monitoring experimental lung injury. *Intensive Care Med* 1998;24:829–836.
30. Frerichs I, Hahn G, Hellige G. Gravity-dependent phenomena in lung ventilation determined by functional EIT. *Physiol Meas* 1996;17(Suppl 4A):A149–A157.
31. Hinz J, Hahn G, Neumann P, Sydow M, Mohrenweiser P, Hellige G,

Burchardi H. End-expiratory lung impedance change enables bedside monitoring of end-expiratory lung volume change. *Intensive Care Med* 2003;29:37–43.
32. Frerichs I, Schiffmann H, Oehler R, Dudykevych T, Hahn G, Hinz J, Hellige G. Distribution of lung ventilation in spontaneously breathing neonates lying in different body positions. *Intensive Care Med* 2003; 29:787–794.
33. Neumann P, Berglund JE, Andersson LG, Maripu E, Magnusson A, Hedenstierna G. Effects of inverse ratio ventilation and positive end-expiratory pressure in oleic acid-induced lung injury. *Am J Respir Crit Care Med* 2000;161:1537–1545.
34. Neumann P, Berglund JE, Mondejar EF, Magnusson A, Hedenstierna G. Effect of different pressure levels on the dynamics of lung collapse and recruitment in oleic-acid-induced lung injury. *Am J Respir Crit Care Med* 1998;158:1636–1643.
35. Kunst PW, Vonk Noordegraaf A, Hoekstra OS, Postmus PE, de Vries PM. Ventilation and perfusion imaging by electrical impedance tomography: a comparison with radionuclide scanning. *Physiol Meas* 1998; 19:481–490.
36. Sipmann FS, Borges JB, Caramez MP, Gaudencio AMAS, Barbas CSV, Carvalho CRR, Amato MBP. Selecting PEEP during mechanical ventilation by using electrical impedance tomography (EIT) [abstract]. *Am J Respir Crit Care Med* 2000;161:A488.
37. Genderingen HR, Vught AJ, Jamsen JRC. Estimation of regional volume changes by electrical impedance tomography during a pressure–volume maneuver. *Intensive Care Med* 2003;29:233–240.
38. Frerichs I, Hinz J, Herrmann P, Weisser G, Hahn G, Dudykevych T, Quintel M, Hellige G. Detection of local lung air content by electrical impedance tomography compared with electron beam CT. *J Appl Physiol* 2002;93:660–666.
39. Victorino JA, Okamoto VN, Borges JB, Janot GF, Tucci MR, Carvalho CRR, Amato MBP. Disturbed regional ventilation in ALI/ARDS assessed by EIT: functional CT validation [abstract]. *Am J Respir Crit Care Med* 2003;167:A618.
40. Dijkstra AM, Brown BH, Leathard AD, Harris ND, Barber DC, Edbrooke DL. Clinical applications of electrical impedance tomography. *J Med Eng Technol* 1993;17:89–98.
41. Grundy D, Reid K, McArdle FJ, Brown BH, Barber DC, Deacon CF, Henderson IW. Trans-thoracic fluid shifts and endocrine responses to 6 degrees head-down tilt. *Aviat Space Environ Med* 1991;62:923–929.
42. Barber DC. Quantification in impedance imaging. *Clin Phys Physiol Meas* 1990;11:45–56.
43. Harris ND, Suggett AJ, Barber DC, Brown BH. Applied potential tomography: a new technique for monitoring pulmonary function. *Clin Phys Physiol Meas* 1988;9:79–85.
44. Harris ND, Suggett AJ, Barber DC, Brown BH. Applications of applied potential tomography (APT) in respiratory medicine. *Clin Phys Physiol Meas* 1987;8:155–165.
45. Nopp P, Harris ND, Zhao TX, Brown BH. Model for the dielectric properties of human lung tissue against frequency and air content. *Med Biol Eng Comput* 1997;35:695–702.
46. Barber DC. A review of image reconstruction techniques for electrical impedance tomography. *Med Phys* 1989;16:162–169.
47. Santosa F, Vogelius M. A backprojection algorithm for electrical impedance imaging. *SIAM J Appl Math* 1990;50:216–243.
48. Hounsfield GN. Computerized transverse axial scanning (tomography): I: description of system. *Br J Radiol* 1973;46:1016–1022.
49. Gattinoni L, Caironi P, Pelosi P, Goodman LR. What has computed tomography taught us about the acute respiratory distress syndrome? *Am J Respir Crit Care Med* 2001;164:1701–1711.
50. Thomas DC, Disall-Allum JN, Sutherland IA, Beard RW. The use of EIT to assess blood volume changes in the female pelvis. In: Holder D, editor. Clinical and physiological applications of electrical impedance tomograph. London: UCL Press; 1993. p. 227–233.
51. Thomas DC, Siddall-Allum JN, Sutherland IA, Beard RW. Correction of the non-uniform spatial sensitivity of electrical impedance tomography images. *Physiol Meas* 1994;15(Suppl 2a):A147–A152.
52. Mantha S, Roizen MF, Fleisher LA, Thisted R, Foss J. Comparing methods of clinical measurement: reporting standards for Bland and Altman analysis. *Anesth Analg* 2000;90:593–602.
53. Bland JM, Altman DG. Measurement error. *BMJ* 1996;312:1654.
54. Hinz J, Neumann P, Dudykevych T, Andersson LG, Wrigge H, Burchardi H, Hedenstierna G. Regional ventilation by electrical impedance tomography: a comparison with ventilation scintigraphy in pigs. *Chest* 2003;124:314–322.
55. Bland JM, Altman DG. Calculating correlation coefficients with repeated observations: I: correlation within subjects. *BMJ* 1995;310:446.
56. Blue RS, Isaacson D, Newell JC. Real-time three-dimensional electrical impedance imaging. *Physiol Meas* 2000;21:15–26.
57. Borges JB, Janot GF, Okamoto VN, Caramez MPR, Barros F, Souza CE, Carvalho CRR, Amato MBP. Is there a true cephalocaudal lung gradient in ARDS [abstract]? *Am J Respir Crit Care Med* 2003;167: A740.
58. Borges JB, Janot GF, Okamoto VN, Barros F, Souza CE, Carvalho CRR, Barbas CSV, Amato MBP. Aggressive recruitment maneuvers assessed by helical CT: is it necessary multiple slices [abstract]? *Am J Respir Crit Care Med* 2002;165:A680.
59. Suki B. Fluctuations and power laws in pulmonary physiology. *Am J Respir Crit Care Med* 2002;166:133–137.
60. Cohen-Bacrie C, Goussard Y, Guardo R. Regularized reconstruction in electrical impedance tomography using a variance uniformization constraint. *IEEE Trans Med Imaging* 1997;16:562–571.
61. Vauhkonen M, Lionheart WR, Heikkinen LM, Vauhkonen PJ, Kaipio JP. A MATLAB package for the EIDORS project to reconstruct two-dimensional EIT images. *Physiol Meas* 2001;22:107–111.
62. Molinari M, Cox SJ, Blott BH, Daniell GJ. Adaptive mesh refinement techniques for electrical impedance tomography. *Physiol Meas* 2001; 22:91–96.
63. Dehghani H, Barber DC, Basarab-Horwath I. Incorporating a priori anatomical information into image reconstruction in electrical impedance tomography. *Physiol Meas* 1999;20:87–102.
64. Avis NJ, Barber DC. Image reconstruction using non-adjacent drive configurations. *Physiol Meas* 1994;15(Suppl 2a):A153–A160.
65. Blott BH, Daniell GJ, Meeson S. Electrical impedance tomography with compensation for electrode positioning variations. *Phys Med Biol* 1998; 43:1731–1739.
66. Edic PM, Isaacson D, Saulnier GJ, Jain H, Newell JC. An iterative Newton-Raphson method to solve the inverse admittivity problem. *IEEE Trans Biomed Eng* 1998;45:899–908.
67. Mueller JL, Siltanen S, Isaacson D. A direct reconstruction algorithm for electrical impedance tomography. *IEEE Trans Med Imaging* 2002;21: 555–559.
68. Tang M, Wang W, Wheeler J, McCormick M, Dong X. The number of electrodes and basis functions in EIT image reconstruction. *Physiol Meas* 2002;23:129–140.
69. Cheng KS, Simske SJ, Isaacson D, Newell JC, Gisser DG. Errors due to measuring voltage on current-carrying electrodes in electric current computed tomography. *IEEE Trans Biomed Eng* 1990;37:60–65.
70. Cook RD, Saulnier GJ, Gisser DG, Goble JC, Newell JC, Isaacson D. ACT3: a high-speed, high-precision electrical impedance tomograph. *IEEE Trans Biomed Eng* 1994;41:713–722.
71. McAdams ET, McLaughlin JA, McC Anderson J. Multi-electrode systems for electrical impedance tomography. *Physiol Meas* 1994;15 (Suppl 2a):A101–A106.
72. Muscedere JG, Mullen JBM, Slutsky AS. Tidal ventilation at low airway pressures can augment lung injury. *Am J Respir Crit Care Med* 1994;149: 1327–1334.
73. Taskar V, John J, Evander E, Robertson B, Jonson B. Surfactant dysfunction makes lungs vulnerable to repetitive collapse and reexpansion. *Am J Respir Crit Care Med* 1997;155:313–320.